Proposal

Measurement of the helicity dependent photoabsorption cross section for the proton to study the Gerasimov-Drell-Hearn sum rule at SPring-8.

T.Iwata (Spokesperson) [1] , S.Fukui, S.Hasegawa, T.Inagaki, N.Inami, T.Kobayashi, L.Wang, S.Nanba,
Nagoya University, Department of Physics
N.Horikawa, I.Daito
Nagoya University, Center for Integrated Research in Science and Engineering (CIRSE)

S.Ishimoto
Institute of Particle and Nuclear Studies (KEK-IPNS)
T.Hasegawa, T.Matsuda
Miyazaki University, Faculty of Engineering
M.Geso
Department of medical radiations sciences, Royal Melbourne Institute of Technology, Australia
D.Menze
Physikalisches Institut, Universität Bonn, Germany
G.Igo, S.Trentalange, V.Ghazikhanian
University of California, Department of Physics, USA
F.Klein
Frorida International University, USA

11 July 2001

Abstract

We propose to measure the total absorption cross section of circularly polarized photons on longitudinally polarized nucleons in the the energy range $1.8< \nu < 2.8$ GeV at SPring-8 LEPS beam line. The measurement, along with the data obtained in other experiments in lower energy range, allows direct experimental verification of the Gerasimov-Drell-Hearn(GDH) sum rule.

[1]position:assistant professor(jyoshu), address: Nagoya University, Department of Physics, Furo-Cho, Chikusa-ku, Nagoya 464, Japan
tel: +81-52-789-2895 fax: +81-52-789-2903
email: iwata@kiso.phys.nagoya-u.ac.jp

1 Introduction

1.1 Gerasimov-Drell-Hearn sum rule

The Gerasimov-Drell-Hearn(GDH) sum rule relates the total absorption cross section of circularly polarized photons on longitudinally polarized nucleons to the statistic properties of the nucleon. The two relative spin configurations, parallel or antiparallel, determine the two absorption cross sections $\sigma_{3/2}$ and $\sigma_{1/2}$. The integral over the photon energy ν of the difference of these cross sections, weighted by the inverse of ν, is related to the mass m and anomalous magnetic moment κ of the nucleon as:

$$\int_{\nu_0}^{\infty}(\sigma_{3/2}-\sigma_{1/2})\frac{d\nu}{\nu}=\frac{2\pi^2\alpha}{m^2}\kappa^2 \tag{1}$$

where ν_0 is the pion threshold and α the fine-structure constant. The GDH values for the proton and the neutron are calculated to be 205 μb and 233 μb, respectively. The GDH sum rule was derived in the 1960's by Gerasimov [1] and independently by Drell and Hearn [2]. They derived it on the bases of important principles such as Lorentz-invariance, gauge invariance, unitarity, causality and the unsubtracted dispersion relation applied to the forward Compton amplitude. Although most of them are believed valid, the application of the unsubtracted dispersion relation is an assumption in physics that means at infinite energy the helicity dependence of the cross section of forward Compton scattering vanishes. The helicity dependence should reflect the spin structure of the nucleon observed at extreme energy. This means the study of GDH sum rule at low energies provides information on the nucleon stucture to be probed at high energies. Another independent derivation using current algebra technique was made almost at the same time by Hosoda and Yamamoto [3] of Osaka University, although it is less well known.

Since the sum rule is a quite fundamental theoretical prediction, its experimental verification has been required for a long time. However, it has not been completed yet due to experimental difficulties. Recently a direct measurement for the proton has been carried out at Mainz [4] in the the energy range $200< \nu < 800$ MeV using a 4π detection system, a circularly polarized tagged photon beam and a frozen spin target. The contribution to the GDH sum rule in this energy range was measured to be $226\pm5(stat)\pm12(sys)\mu$b. Taking account of the contribution of -30μb [7] from unmeasured low energy region(ν <200MeV), the measured value is consistent with the GDH sum rule prediction within the experimental errors. However, the running GDH integral,

$$\int_{200MeV}^{\nu}(\sigma_{3/2}-\sigma_{1/2})\frac{d\nu'}{\nu'}, \tag{2}$$

has a tendency to increase even around the energy of 800 MeV as displayed in Fig. 1. And the data above 400 MeV are not well reproduced by theoretical models: HDT [5], SAID [6], and UIM [7]. These lead to the importance of measurements in higher energy ranges in spite of the factor $1/\nu$ in the sum rule.

The GDH sum rule has attracting interests in connection with the spin structure of the nucleon. Polarized deep inelastic scattering experiments measuring the spin dependent structure functions $g_1(x)$, have led to an interesting result; a small amount of the nucleon

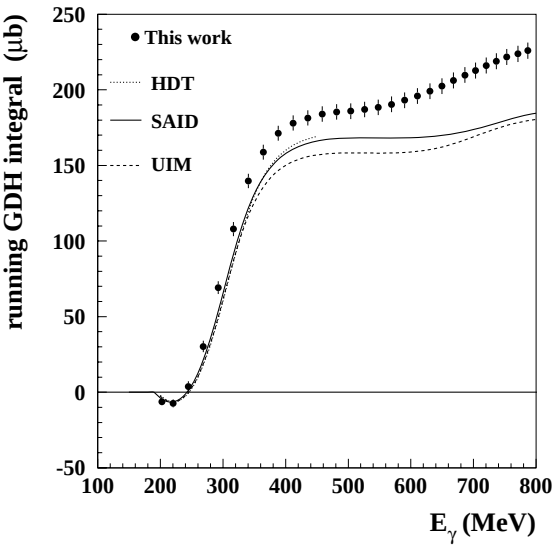

Figure 1: The running GDH integral obtained in the Mainz experiment starting at 200 MeV is compared to the model predictions. Only statistical errors are shown.

spin is carried by quarks, which is often referred to as "Spin Crisis". It is pointed out [8] that a function defined with the $g_1(x)$,

$$I(Q^2) = \frac{2m^2}{Q^2}\int_0^1 g_1(x, Q^2)dx, \tag{3}$$

is related to the the GDH sum rule at $Q^2 = 0$ as follows.

$$I(0) = -\frac{\kappa^2}{4}, \tag{4}$$

because the photoabsorption reaction by real photons is the limit of the deep inelastic scattering for $Q^2 \to 0$.

The experimental values are obtained at different Q^2 as shown in Fig. 2. They are located close to zero. While, the predicted values by the GDH sum rule are located far from 0; $I_p(0) = -0.8$ and $I_n(0) = -0.9$. In particular, all the experimental values for $I_p(Q^2)$ are positive although the predicted value at $Q^2 = 0$ is negative. This suggests that a strong Q^2 dependence in the small Q^2 region exists, if the GDH sum rule prediction is satisfied. On the other hand, the difference, $I_p(Q^2) - I_n(Q^2)$, corresponding to the Bjorken sum rule [9] which is well verified experimentally in high Q^2 region, seems to approach the predicted value by the GDH sum rule.

Some theoretical calculations for the GDH integral have been made in the past few years as shown in Table.1.1. Most of them are based on the multipole analyses for the existing single pion photoproduction data. In Ref.[15], an additional contribution due to multihadron production processes was phenomenologically evaluated using a Regge-type approach. Ref.[16] uses extended current algebra. It is notable that most calculations, with the exception of Ref. [15], give an opposite sign to the GDH sum rule for I_{p-n}^{GDH}

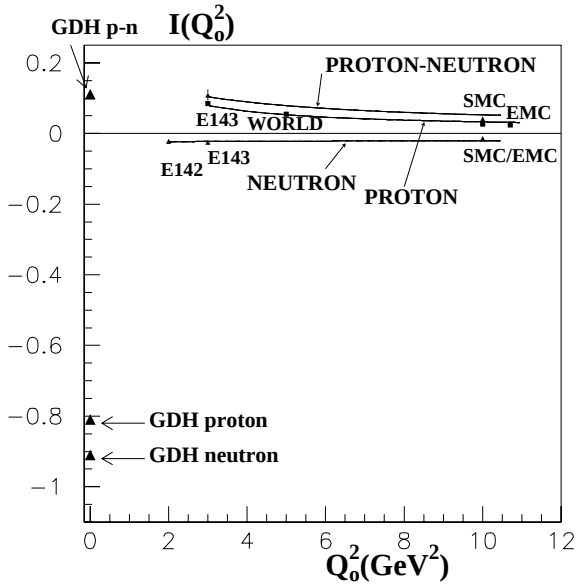

Figure 2: $I(Q^2)$ for proton, neutron and proton-neutron along with the predictions by the GDH sum rule at $Q^2 = 0$. The curves are eye guides.

contribution.

2 Measurement of the helicity dependent photoabsorption cross section at SPring-8.

A circularly polarized photon beam is available at SPring8 LEPS facility by backward Compton scattering of a laser light off the circulating electrons of 8 GeV in the storage ring. The energy range currently available is up to 2.4 GeV with an Ar-laser of λ =351 nm. It can be extended to 2.8 GeV using an Ar-laser of λ =275 nm. We propose to measure the helicity dependent photoabsorption cross sections for the proton using the LEPS facility in the energy ranges 1.8< ν <2.4GeV (first phase) and 2.3< ν <2.8GeV (second phase). The difference of the two helicity dependent photoabsorption cross sections,

$$\Delta\sigma = \sigma_{3/2} - \sigma_{1/2} \tag{5}$$

will be measured. Our goal is to obtain the GDH integral in the measured energy ranges allowing to verify the GDH sum rule.

The experiment requires a 4π detection system and a polarized target. The former one can be made mostly by reassembling the apparatus currently available at LEPS facility. Only a few detectors should be newly constructed. As for the polarized target which is essential for the experiment, technical developments have been carried out by Nagoya

Table 1: Various calculations for the GDH integral.

	I_p^{GDH} (μb)	I_n^{GDH} (μb)	I_{p-n}^{GDH} (μb)
GDH sum rule	205	233	-28
Karliner [10]	261	183	78
Workman-Arndt [11]	257	189	68
Burkert-Li [12]	203	125	78
Sandorfi et. al. [13]	289	160	130
Drechsel-Krein [14]	261	180	81
Bianchi-Thomas [15]	207 $\pm$ 23	226 $\pm$ 22	-19$\pm$ 37
Extended Current Algebra [16]	294	185	109

group in their polarized target test facility at Nagoya. A polarized target system to fit the experiment should be constructed.

2.1 General Consideration of the Measurement

The physical asymmetry A for the γp process is defined as

$$A = \frac{\Delta\sigma}{2\sigma^0}, \tag{6}$$

with the unpolarized γp cross section $\sigma^0 = (\sigma_{3/2} + \sigma_{1/2})/2$. While the asymmetry directly obtianed in the experiment is

$$\epsilon = \frac{N_{3/2} - N_{1/2}}{N_{3/2} + N_{1/2}}, \tag{7}$$

where $N_{3/2}$ and $N_{1/2}$ are the numbers of hadronic events for the different helicity configurations of the photon beam and the target. The physical asymmetry A is expressed with ϵ as

$$A = \frac{1}{P_B P_T f} \cdot \epsilon, \tag{8}$$

where P_B and P_T are the beam and the target polarizations, f is the dilution factor of the target which means the fraction of polarizable protons over all the nucleons in the target. f is defined rigorously as a fraction of the events associated with the polarized protons in the target over the all hadronic events, thus, expressed as

$$f = \frac{n\sigma^0}{n_{tot}\sigma_{tot}}. \tag{9}$$

n and σ^0 are the number of the polarizable protons in the target and the unpolarized total cross section for the γp process, respectively. n_{tot} and σ_{tot} are the number of all the nucleons in the target and the total cross section for the target per nucleon, respectively. The denominator of the right side in eq.9 is further expressed as

$$n_{tot}\sigma_{tot} = n\sigma^0 + n_{bg}\sigma_{bg}, \tag{10}$$

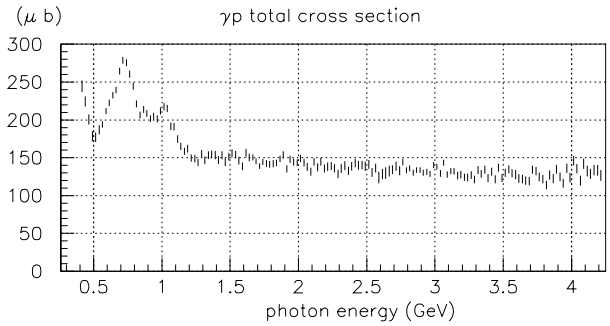

Figure 3: Total photoabsorption cross section as a function of photon energy.

where n_{bg} and σ_{bg} are the number of unpolarizable nucleons inside background nueclei(unpolarizable) and the total cross section per nucleon for the nucleus, respectively. The total cross section for the γp process, $\sigma^0 \sim 130$ μb has been measured with errors of about 4 % [17] as shown in Fig. 3. For background nuclei data are available [18] with slightly larger errors; in the case of carbon, the errors are about 5 %. Using these data, one can evaluate the dilution factor f with about 6 % accuracy.

Then, from eq.6 and eq.8, the difference of the helicity dependent cross sections is given by

$$\Delta\sigma = \frac{2\sigma^0\epsilon}{P_T P_B f}. \tag{11}$$

The GDH sum rule for proton reads

$$\int_{\nu_0}^{\infty} \frac{\Delta\sigma}{\nu} d\nu \sim 200\mu b. \tag{12}$$

Now, we define the regional GDH integral as

$$I_{GDH}(\nu_1, \nu_2) = \int_{\nu_1}^{\nu_2} \frac{\Delta\sigma}{\nu} d\nu \tag{13}$$

for the energy region from ν_1 to ν_2. Assuming $\Delta\sigma$ stays approximately constant, the uncertainty for $I_{GDH}(\nu_1, \nu_2)$ may be expressed as

$$\delta I_{GDH}(\nu_1, \nu_2) = \delta(\Delta\sigma) \log \frac{\nu_2}{\nu_1} \tag{14}$$

In order to test the GDH sum rule with an accuracy of 5% , namely $\sim$10 μb for the GDH integral,

$$\delta I_{GDH}(\nu_1, \nu_2) < 10\mu b, \tag{15}$$

is required. This leads to $\delta(\Delta\sigma) \sim 20\mu$b for ν_1 =1.8 and ν_2 =2.8 GeV.

2.2 Experimental apparatus

2.2.1 Photon beam

The photon beam at SPring-8 LEPS is produced by backward Compton scattering(BCS). The maximum photon energy depends on the the energies of the laser photon and the electron as

$$\nu_{max} = E_e \frac{\alpha}{1+\alpha}, \tag{16}$$

with $\alpha = 4E_e\epsilon_l/m^2$ where E_e=8GeV and m are the energy and the mass of the electron, ϵ_l is the energy of the laser photon. With laser beam of λ =351 nm(3.53 eV), one obtains the maximum photon energy of 2.4 GeV. For λ =275nm (4.49 eV), it extends to 2.8GeV.

The divergence of the photon beam is rather small due to Lorenz boost by the high energy electron: 70 μrad at 2.4 GeV. Even taking account of the actual emittance of the electron beam of $7 \cdot 10^{-7} m \cdot rad.$, the divergence is expected to be about 100 μrad. This gives a small beam spot at the target point: σ_x=3 mm and σ_y=1.5 mm.

The intensity of the photon beam is given by electron-laser interaction length L , energy ϵ_l per laser photon, laser power P_l , and stored electron current I_e as;

$$Y(sec^{-1}) = \frac{(2.60) I_e(amps) P_l(watts) \sigma(mb) L(cm)}{\epsilon_l(eV) S(cm^2)}, \tag{17}$$

where σ is the laboratory cross section for the BCS process integrated over the photon beam definition angle, and S is the cross sectional area of the laser beam. When a laser beam from an Ar-laser($\lambda = 351nm$, $\epsilon_l = 3.53eV$) providing 2W, is focussed into the area of $\phi 1mm$, $1.6 \cdot 10^6 s^{-1}$ photons are expected for $I_e = 100mA$ and $L = 200cm$. However, the currently available intensity is about 8.0$\times$ $10^5\gamma$/s due to limited transmission of the laser beam.

The energy of the photon is determined in the energy range above 1.5 GeV by the tagging system composed of a silicon micro-strip detector. The energy resolution of 15 MeV is typically obtained.

Circular polarization of the laser is transferred to the scattered photon with the polarization transfer efficiency P_{eff} which is a function of the energy of the produced photon as shown in Fig. 4. It is $P_{eff} = -100\%$ at the maximum photon energy point and approaches to 0 % as the energy decreases. The averaged efficiencies in the energy ranges in which our measurement is proposed are $< P_{eff} >= -80\%$ for 1.8$< \nu <$2.4 GeV and $< P_{eff} >= -60\%$ for 2.3$< \nu <$2.8 GeV.

Polarization of the laser beam will be changed every hour by rotating a 1/4 λ-plate. The polarization is monitored by the polarimeter installed at the laser-beam-end with an accuracy of 0.1 % . From the polarization of the laser beam and the energy of the produced photon given by the tagging system one can calculate the polarization of the photon. The uncertainty of the polarization is mainly caused by the energy resolution(15 MeV) of the tagging system. We expect the accuracy of $\sim \delta P_B/P_B = 1\%$.

2.2.2 Polarized target

A polarized target using dynamic nuclear polarization(DNP) technique will be applied for the proposed experiment. This type of targets requires paramagnetic centers in the

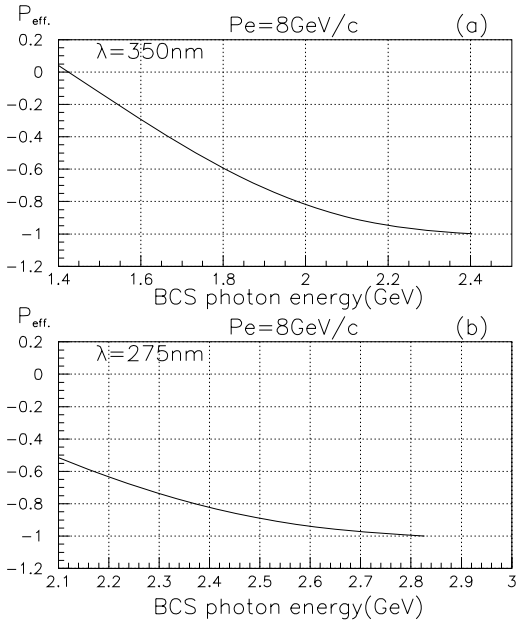

Figure 4: Polarization transfer efficiency as a function of the scattered photon energy for (a)λ =350 nm and (b) λ =275 nm.

vicinity of the nuclei to be polarized. The most convenient way to realize this is doping the target with a small fraction of free radical which contains free electrons. And it is kept under a homogeneous high magnetic field(typically 2.5 T) at a temperature below 0.3K. Microwave with frequencies set at slightly below or above the frequency of electron spin resonance, will lead to positive or negative target polarization. Polarization measurement is made by NMR technique. This type of target has been developed and reliably used in many experiments for more than 30 years.

A super-conducting solenoid magnet with a warm bore of 60 cm in diameter will be employed to produce a 2.5 T field. Such a large bore enables to install detectors at the places close to the target. Field homogeneity of $\Delta B/B \sim 10^{-4}$ is obtained over a volume of $50mm \times \phi 30mm$. This magnet is equipped with a GM refrigerator and allows an operation without liquid helium. It was purchased in 2000 using a budget of RCNP.

A dilution refrigerator for the polarized target should give a large cooling power as much as several mW at around 0.3K. Such a refrigerator is not commercially available, so that one should design and construct it. However, this is connected to high costs and is time consuming. We will try to borrow the old dilution refrigerator [19] which had been used for the KEK polarized target. If it is not successful, we will construct a new refrigerator based on the same design. The dilution refrigerator requires a gas circulation system which includes large pumps. This system should be newly prepared.

We will use polyethylene -CH_2- as target material. The dilution factor is about 0.14. It has a good property different from other target materials. It can be prepared and fabricated easily at room temperature. For this property, the thickness of the target can be precisely controlled and accurately evaluated. This is important in particular for

consistency check in measurements of absolute cross sections. Polyethylene foils of 100 μm thickness are doped with a free radical called TEMPO (2,2,6,6-methyl-piperidine-oxyl) which is a remarkable stable material. 400 sheets of the foils will be stacked to form a target with a cylindrical shape with ϕ20 mm and a thickness of 40 mm. The polyethylene polarized target has been developed by the Nagoya group; they have obtained polarization of 60 % so far and expect 80 % in future.

Polarization is measured by a NMR system consisting of a RF-Q meter, a frequency synthesizer and an ADC board. Calibration of the NMR system is performed observing a thermal equilibrium signal at a temperature of 1K and in a 2.5T field. The accuracy of the polarization is expected to be $\delta P_T/P_T = 3\%$. The uncertainty is dominantly caused by the measurement of the thermal equilibrium signal and the uncertainty of the temperature measurement around 1K.

The microwaves for a polarization enhancement are produced by an impatt diode oscillator having the maximum output power of 300 mW at 70 GHz.

Nagoya group has a responsibility to provide the essential parts of the NMR and the microwave systems.

2.2.3 Detection System

The proposed experiment will use a 4π detection system which allows to detect all the charged particles and gamma rays produced in the reaction. The system is shown in Fig.5. It is divided into two sections: the 'central section' consisting of detectors surrounding the target inside the magnet bore and the 'forward section' for particles emitted in the forward direction.

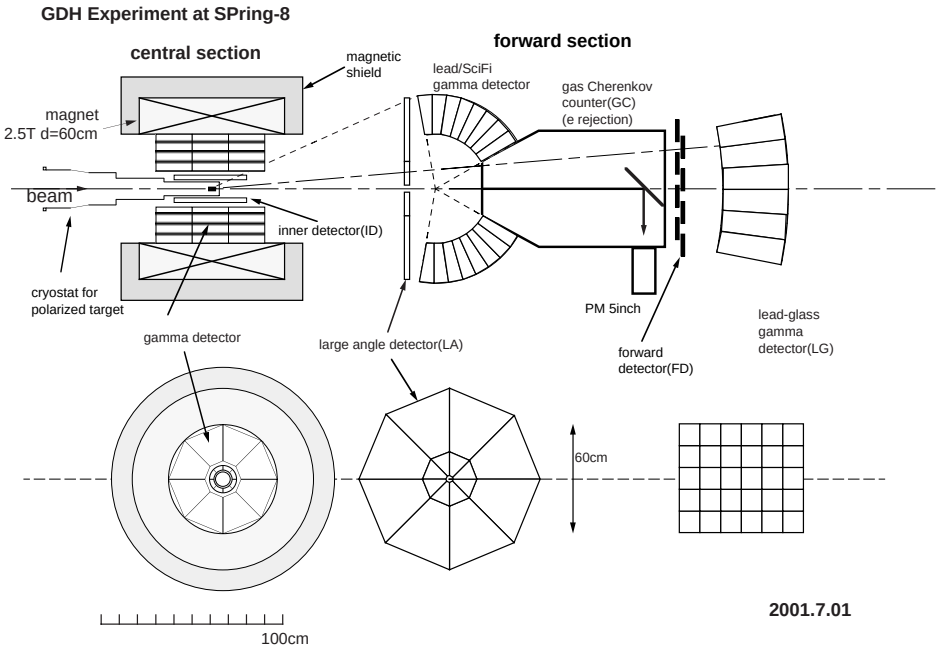

Figure 5: Detection system.

The 'central section' includes the 'inner detector(ID)' for charged particle detection to

be placed close to the target and the 'gamma detector' installed into the gap between the ID and the inner surface of the magnet. Both detectors should fulfil specific requirements: (1) they are installed into the narrow space inside the bore of the magnet, (2) they should function in the magnetic field of 2.5T, (3) detection efficiencies should be high even with limited thickness and (4) insensitive area should be as narrow as possible not to loose 4π geometry. These requirements lead to a choice of detectors using plastic scintillators with a readout of wave length shifter(WLS) fibers. The WLS fiber is embedded into a groove on the surface of the plastic scintillator and its end is connected to a transparent light guiding fiber to lead to a photomultiplier. This type of detectors allows, employing long light guiding fibers, to place photomultipliers at a distance far from the magnetic field. We will apply this technique to the 'gamma detector' and also to the ID. The ID has a pipe-like shape made of plastic scintillator as shown in Fig.6 with the outer diameter of 150mm, a thickness of 25mm and a length of 400mm. It is divided into 10 sections along the axis and 8 sectors in the azimuthal angle resulting in a module. Each module, has four grooves on its outer surface; two spiral ones and two straight ones along the axis. The modules of the neighboring section are rotated by half a module so that the grooves are smoothly connected to the ones of other modules in the neighboring section. WLS fibers are embedded in these grooves. This configuration leads to three groups of readout: U(8 channels), V(8 channels) in spiral and ϕ(16 channels) along the axis.

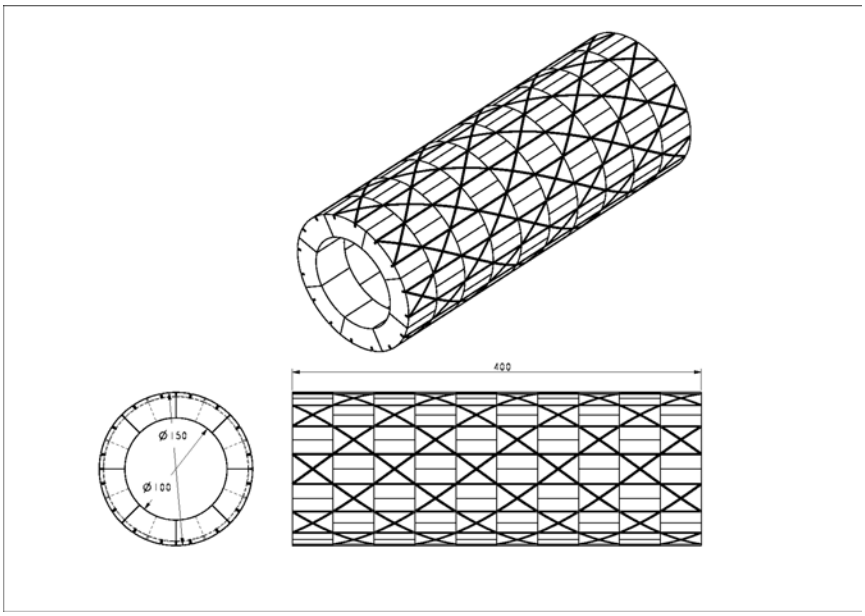

Figure 6: The 'inner detector'.

The 'gamma detector' has a trapezoidal cross section and each module covers a 1/8 sector in the azimuthal angle as shown in Fig.7. It consists of 18 sampling layers of different areas. Each layer consists of a lead tile of 1.6 mm thickness and a scintillator tile of 8 mm thickness. Grooves were etched on the surface of the scintillator tiles. Two different shaped grooves are formed: race-track and S type. The first type is adopted for the large area tiles. The groove depth around 2.6 mm allows two turns of the WLS fiber of 1mm diameter to be installed in the tile. The second type, S type, allows only a single

trace through the S-shaped groove of 1.6 mm in depth. This type is adopted for the first five tiles. The end of the WLS fiber is glued to the light guiding fiber (3m long). The other end of the the light guiding fiber is directly attached to a photomultiplier.

A prototype of the 'gamma detector' has been fabricated and tested [20] using minimum ionizing particles, electrons and gamma rays. The results of the test were compared with those obtained by a Monte Carlo simulation. A typical spectrum obtained for a gamma ray at the energy of 630 MeV is displayed in Fig.8. The detection efficiency for gamma rays was evaluated based on the simulation and also measured with a tagged photon beam of LNS in Tohoku University as shown in fig. 9. It is found to be higher than 90% at energies above 50 MeV.

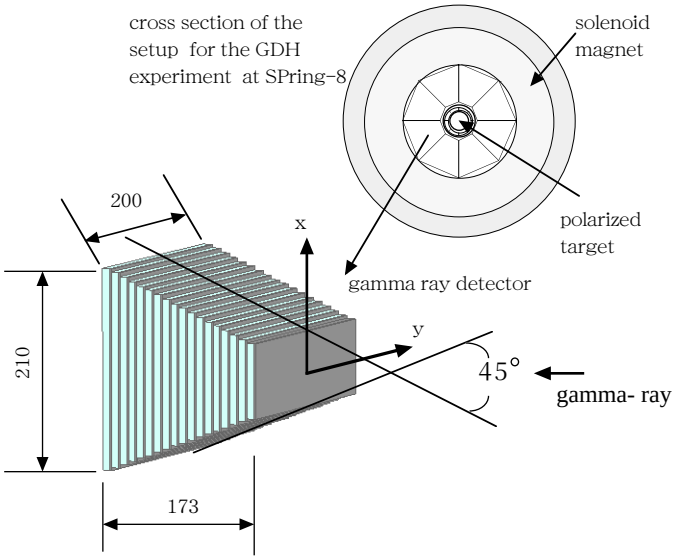

Figure 7: The 'gamma detector' in the central section.

The detectors in the 'forward section' are a 'large angle detector', a 'lead/SciFi gamma detector', a 'gas Cherenkov counter', a 'forward detector' and a 'lead-glass gamma detector'. The 'large angle detector(LA)' and the 'forward detector(FD)' are hodoscopes made of plastic scintillator. The hodoscope LA will be newly constructed, while, the hodoscope FD can be replaced by a part of the TOF wall currently employed in the LEPS spectrometer.

The hodoscope LA is followed by the 'lead/SciFi gamma detector(LS)' which is the backward gamma detector constructed for the LEPS facility. It has 252 modules consisting of scintillation fibers placed between wavy lead plates. The scintillation light is read by photomultipliers. However, the stray field about 150 Gauss from the solenoid magnet prevents the photomultipliers from functioning. Thus, they have to be replaced by special photomultipliers which are resistive to the magnetic field.

Between the LS and the FD, a 'gas Cherenkov counter(GC)' will be placed to veto electromagnetic showers. The radiator gas will be CO_2 at atmospheric pressure giving a refractive index of n=1.00043 which corresponds to threshold momenta for π of 4.9 GeV/c and for electrons of 17.5MeV/c. The electromagnetic showers are caused with the cross section two orders of magnitude larger than that of the hadronic event. We

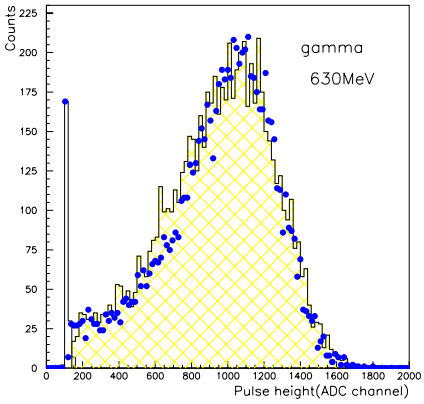

Figure 8: The pulse height distribution for gamma rays at 630MeV (histogram) in comparison with a Monte Carlo simulation(closed circles). The fraction of the events in the hatched area to the total events gives the detection efficiency of 97.1 ± 0.2 %.

would like to suppress them by 10^{-4} in the trigger level. This counter is required to have detection efficiency of more than 99.99 % for an electromagnetic shower event. Since one electromagnetic shower contains at least e^- and e^+ tracks in average, the efficiency for a single track detection should be approximately more than 99 %. A prototype of the counter has been fabricated and tested [21] using electrons at an energy of 300 MeV. An efficiency of 99.6 % for a single track was obtained with a threshold of 1 photo-electron level. A Monte Carlo simulation taking account of the value gave the efficiency for the shower event of 99.89 ± 0.094 %. This is almost satisfactory for the proposed experiment. Triggered shower events, although of which amount is a few percent of the hadronic events, will be discarded in the off-line analyses using the data of forward detectors.

Most downstream the 'lead-glass gamma detector(LG)' is installed for which we will employ 30 lead-glass blocks used in the TOPAZ experiment in TRISTAN at KEK. Each block has 20 radiation length.

This detection system totally covers the laboratory scattering angle from 0.3° to 146° resulting in the geometrical acceptance of $4\pi \times 92\%$. The loss in the acceptance is mainly caused at large angles where low energy particles are anticipated. When they are emitted at large angles, due to energy and momentum conservation, high energy particles are expected in forward direction. They are detected by the forward detectors. Therefore, the detection efficiency for hadronic events does not suffer from the loss in the acceptance.

2.3 Counting Rate

We evaluate the counting rates for the polyethylene target with a thickness of 4cm and the total photon intensities for the full spectrum of $8.0 \times 10^5 \gamma s^{-1}$ in the first phase and $8.0 \times 10^4 \gamma s^{-1}$ in the second phase. They are listed in Table 2 along with those of electromagnetic shower events.

2.4 Errors and beam time request

The origins of systematic errors affecting on $\Delta\sigma$ are uncertainties of the target polarization ($\delta P_T/P_T \approx 3\%$), the beam polarization ($\delta P_B/P_B \approx 1\%$), the detector acceptance ($\sim 2\%$), target dilution factor ($\delta f/f \approx 6\%$), and the total cross section ($\delta\sigma^0/\sigma^0 \approx 4\%$). These values lead to the total systematic error of 8%. Since the $\Delta\sigma$ has the restriction, $-2\sigma^0 < \Delta\sigma < 2\sigma^0$ with $\sigma^0 \sim 140\mu$b, the systematic error leads to $\delta(\Delta\sigma) < 22\mu$b.

The data taking period needed to obtain a certain statistical error for $\Delta\sigma$ is given by;

$$T = (\frac{1}{P_T P_B f})^2 (\frac{2\sigma^0}{\delta(\Delta\sigma^0)})^2 \frac{1}{2\dot{N}_{had}}, \tag{18}$$

where $\dot{N}_{had}$ is the hadronic event rate per 100 MeV energy bin. Requiring $\delta(\Delta\sigma)$ to be one order of magnitude smaller than the maximum expected systematic error, namely, $\delta(\Delta\sigma) \sim 2\mu$b and for $P_T = 0.7$, $P_B = 0.8$, $f = 2/14$, $\dot{N}_{had} \sim 13$/sec in the first phase measurement, the data taking period needed is 33 hours. As for the second phase measurement, with $\dot{N}_{had} \sim 1$/sec, it is 425 hours(∼18 days). These periods are only for data taking. Additional periods are needed in the beam time for a polarization reversal(8 hours/reversal) which will be done every 12 hours, NMR calibration(5 hours), runs for calibration(10% of the data taking time) , runs with an empty target(10% of the data taking time) and runs with a carbon target(10% of the data taking time). In the preparation stage, we require one week for the detector tuning. The summary of the beam time request is shown below.

beam time request

phase	first phase time(in hours)	second phase time(in hours)
data taking	33	425
polarization reversal	15	180
NMR calibration	10	20
run for calibration	3	42
empty target run	3	42
carbon target run	3	42
total	62	751(∼31 days)

3 Cost Estimate

The cost estimates for the parts of the apparatus that have to be either bought or newly built are given in this section.

Cost estimates

item		cost(10k yen)	
∗	polarized target		
	new dilution cryostat(modification of KEK-DR)	1,500(300)	
	pumps	1,500	
	^{3}He gas circulation sytem	1,000	
	He dewars	300	
	^{3}He gas(200L)	100	
	microwave parts	100	
	NMR system	200	
	plat form	200	
		sub total	4,900(3,700)
∗	operation of polarized target		
	Liquid ^{4}He (100L/day×30 days)	300	
	Liquid N_2 (300L/day)	50	
		sub total	350
∗	detection system		
	construction of ID	50	
	PMs for ID(2 PM with multi anodes)	50	
	construction of 'gamma detector'	200	
	PMs for 'gamma detector'	600	
	PMs for LA	320	
	PMs for 'lead/SciFi gamma detector' (252 PMs)	5,000	
	gas Cherenkov counter	100	
	frames for the detectors	500	
	installation of 'lead-glass gamma detector'	300	
		sub total	7,120
		grand total	12,370(11,170)

4 Collaborator list

name	affiliation	position
Takahiro Iwata	Nagoya Univ.	Assis. Prof.(Jyoshu)
Shuji Fukui	Nagoya Univ.	Prof. emeritus
Shoichi Hasegawa	Nagoya Univ.	DC student
Takaya Inagaki	Nagoya Univ.	MC student
Noriaki Inami	Nagoya Univ.	MC student
Tomohiro Kobayashi	Nagoya Univ.	MC student
Wang Li	Nagoya Univ.	MC student
Susumu Nanba	Nagoya Univ.	MC student
Naoaki Horikawa	Nagoya Univ.	Prof.
Izuru Daito	Nagoya Univ.	Assis. Prof.(Jyoshu))
Shigeru Ishimoto	KEK-IPNS	Assis. Prof.(Jyoshu)
Takeo Hasegawa	Miyazaki Univ.	Prof.
Tatsuro Matsuda	Miyazaki Univ.	Associ. Prof.
Moshi Geso	Royal Melbourne Institute of Technology	lecturer
Dietmaer Menze	Univ. Bonn	Senior Researcher
George Igo	UCLA	Prof.
Steve Trentalange	UCLA	Post Doctral Fellow
Vahe Ghazikhanian	UCLA	Post Doctral Fellow
Franz Klein	Frorida International Univ.	Post Doctral Fellow

References

[1] S.B.Gerasimov Yad.Fiz. 2(1965)598, Sov.J.Nucl. Phys. 2 (1996) 430.

[2] S.D.Drell and A.C.Hearn, Phys.Rev.Lett. 16 (1966) 908.

[3] M.Hosoda and K.Yamamoto, Prog. Theo. Phys., 16, 908 (1966).

[4] J.Ahrens et al., Phys. Rev. Lett. 87, 022003 (2001).

[5] O.Hanstein et al., Nucl. Phys. A632, 561 (1998).

[6] R.A.Arndt et al., Phys. Rev. C 53, 430 (1996); recent SAID(GWU) solution SP01, R.A. Arndt, I.Strakovsky, and R.Workman (to be published).

[7] D.Drechsel et al., Nucl. Phys. A645, 145 (1999).

[8] M.Anselmino, B.L.Ioffe and E.Leader, Sov.J.Nucl.Phys. 49 (1989).
V.Burkert and B.L.Ioffe, Phys. Lett. B296 (1992) 223.
V.Burkert and B.L.Ioffe, JETP 105 1153 (1994). 49, 136 (1989).

[9] J.D. Bjorken, Phys. Rev. 148 (1966) 1467;
Phys. Rev. D1 (1970) 1376.

[10] I.Karliner, Phys.Rev. D7, (1973) 2717.

[11] R.L.Workman and R.A.Arndt, Phys. Rev. D45 (1992) 1789.

[12] V.Burkert and Zh.Li, Phys. Rev. D47 (1993) 46.

[13] A.M.Sandorfi, C.S.Whisnant and M.Khandaker, Phys. Rev. D50, (1994) 11.

[14] D.Drechsel and G.Krein, Phys. Rev. D 58, 1116009 (1998).

[15] N.Bianchi and T.Thomas, Phys. Lett. B 450, 439 (1999).

[16] L.N.Chang, Y.Liang and R.L.Workman, Phys.Lett. B329 (1994) 514.

[17] T.Armstrong et. al, Phys. Rev. D5 (1972) 1640.

[18] V.Muccifora et al., preprint nuc-exl9810015.

[19] S.Ishimoto et al., Jpn.J.Appl.Phys., 28 (1989) 1963

[20] I.Daito et al., to be published in Nucl.Instrum. and Meth. A.

[21] H.Ichihara, Master Thesis in Department of Physics, Nagoya University,(2000). Refer to http://plib.phys.nagoya-u.ac.jp/CONSTRUCTION/preprint-center/

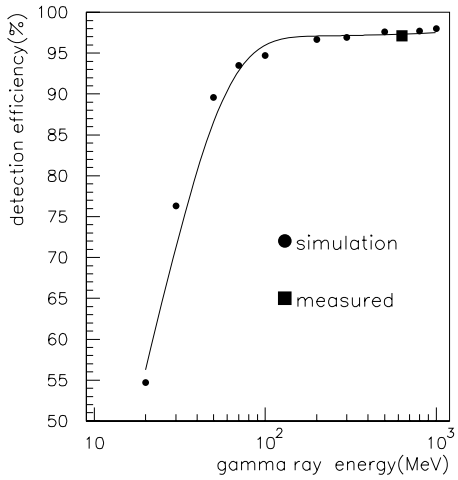

Figure 9: The detection efficiency of the 'gamma detector' for gamma rays as a function of their energy. The closed square is the measured value. The closed circles are obtained in the simulation. The solid line is an eye guide.

Table 2: Expected counting rates: $\dot{N}_\gamma$; photon intensity, $\dot{N}_{had}$; counting rate for hadronic events, $\dot{N}_{shower}$; counting rate for electromagnetic shower events. The efficiency of the 'gas Cherenkov counter for an electromagnetic shower is assumed to be 99.99 % (rejection power is 10^{-4}).

phase	first phase		second phase	
laser wave length	351 nm		275 nm	
$\nu(GeV)$	1.8 - 2.1	2.1 - 2.4	2.3 - 2.6	2.6 - 2.8
P_γ (polarization)	80 %	95 %	80 %	95 %
$\dot{N}_\gamma(s^{-1}/100\text{MeV})$	3.2×10^4	4.1×10^4	3.0×10^3	3.0×10^3
$\dot{N}_\gamma(s^{-1}$, full spectrum)	8.0×10^5		8.0×10^4	
σ^0 (μb)	~ 145	~ 135	~ 130	~ 130
$\dot{N}_{had}(s^{-1}$, full spectrum)	270		25	
$\dot{N}_{had}(s^{-1}$, measured region)	75		4.9	
$\dot{N}_{had}(s^{-1}/100MeV)$	11	14	0.9	1.1
$\dot{N}_{shower}(s^{-1}$, full spectrum)	4×10^4		2×10^3	
$\dot{N}_{shower}(s^{-1}/100\text{MeV})$	2.0×10^3	2.4×10^3	2.5×10^2	2.5×10^2
$\dot{N}_{shower}(s^{-1}/100\text{MeV})$ triggered with GC	0.2	0.24	0.017	0.017